ADVANCED SENSOR RESEARCH Open Access
www.advsensorres.com

Corrole Polymers as a Novel Materials for Room Temperature Resistive Gas Sensors

Lorena Di Zazzo, Ilaria di Filippo, Lorenzo Guido, Gabriele Magna, Larisa Lvova, Fabrizio Caroleo, Manuela Stefanelli, Leonardo Duranti, Sara Nardis, Corrado Di Natale, and Roberto Paolesse**

Corroles, a family of contracted porphyrinoids, exhibit broad chemical interactions, undergo straightforward synthetic preparation and functionalization, and enable versatile thin film deposition. These attributes render them promising candidates for use in chemical sensors. Nevertheless, the inherently limited conductivity of corrole solid films constrains their application in mass and optical sensors. Despite this impediment, there is a great interest in matching the sensitive properties of the corrole with the features of facile miniaturization and integration into low-cost electronic circuits. This work explores the possibility of directly and simply depositing conductometric polymeric films of [5,10,15-(4-aminophenyl)corrolato] copper onto interdigitated electrodes. Remarkably, the electropolymerization protocol allows the selection of the semiconductive nature (p- or n-type) of these films, yielding two distinct sensor types: the former exhibiting high sensitivity and selectivity toward nitrogen monoxide (NO) with a slight influence of relative humidity and the other manifesting a broad spectrum of sensitivities. This breakthrough lays the foundation for developing miniaturized conductometric gas detectors, nonlinear conductometric sensing elements, and electronic nose platforms based on polycorroles.

1. Introduction

The demand for high-performance gas sensors is continuously growing, especially prompted by prominent technological concepts like wireless electronics, flexible support, and wearable devices. Gas sensors in these fields are expected to boost the capabilities of strategic applications such as those aimed at monitoring physiological parameters and environmental conditions.[1] These emerging use cases require devices that, besides the self-evident sensitivity and selectivity, are small, cost-effective, low-power, and easily integrated into electronic platforms. These demands often conflict with the properties of many state-of-the-art sensors. For example, metal-oxide semiconductors might match the requirements for integrated gas sensors, but their high operating temperatures make them unsuitable for low-power applications.[2] On the other hand, certain molecular materials possess exceptional sensing properties, but their scarce conductivity necessitates a more complicated, voluminous, and power-consuming electronic interface setup to accommodate devices based, for example, on optical or mass-sensing transduction.

This drawback is clear in the case of porphyrin and corrole complexes. These receptors comprise three elements: a pyrrolic aromatic ring, a metal complex at the core, and peripheral substituents.[3,4] Changes in each of these elements offer options for customization. For instance, the distinct molecular framework of porphyrins and corroles produces two different aromatic pathways, which strongly influence the coordination chemistry of the numerous metals that may be incorporated in the core of their aromatic rings.[5,6] Additionally, a wide array of molecular motifs can be appended at the peripheral positions[7] to tailor molecular structures with specific chemical interaction properties.

On the other hand, molecular assemblies of porphyrinoids are generally poorly conductive, which has confined their use in sensors based on mass and optical transducers.[8] A widely explored strategy to form conductive sensors with these macrocycles consists of grafting these dyes onto conductive substrates, including metal oxides,[9] graphene,[10] carbon nanotubes,[11] and conductive polymers.[12]

This paper explores an alternative approach to producing conductive sensors based on porphyrinoids straightforwardly by exploiting the properties of electropolymerized corroles

L. D. Zazzo, I. di Filippo, G. Magna, L. Lvova, F. Caroleo, M. Stefanelli, L. Duranti, S. Nardis, R. Paolesse
Department of Chemical Science and Technologies
University of Rome Tor Vergata
via della Ricerca Scientifica 1, Rome 00133, Italy
E-mail: roberto.paolesse@uniroma2.it
L. Guido, C. Di Natale
Department of Electronic Engineering
University of Rome Tor Vergata
viale del Politecnico, Rome 00133, Italy
E-mail: dinatale@uniroma2.it

The ORCID identification number(s) for the author(s) of this article can be found under https://doi.org/10.1002/adsr.202400005

DOI: 10.1002/adsr.202400005

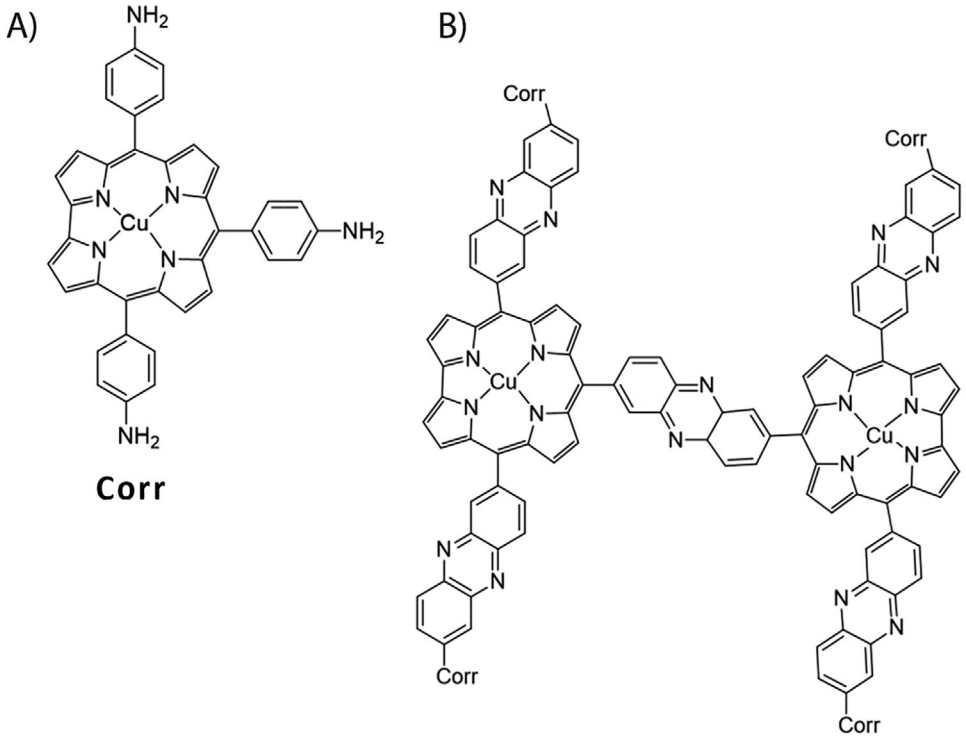

Figure 1. A) Structure of corrole and B) corrole polymer.

characterized by electron-active substituents. This approach is not strictly new since it has already been investigated to prepare electroassisted conductive polymers based on porphyrinoids.[13–16] A typical example is the electrochemical oxidation of 5,10,15,20-tetrakis-(4-aminophenyl)porphyrins or 5,10,15-tris-(4-aminophenyl)corroles, which leads to the formation of different types of linkers as the phenazine bridge.[14,15] However, these materials have been mainly used for the electrochemical detection of species in solutions or as electrocatalysts for the oxygen reduction reaction,[16] while to the best of our knowledge, there are no examples of gas sensors based on this class of materials. In a recent paper, we reported the first synthesis of copper polycorroles and their integration into organic heterostructures in combination with a molecular semiconductor.[17] These heterojunctions benefit from the high interfacial charge transport at the organic–organic junction, owing to the accumulation of mobile charges.[18] We decided to investigate further the exploitation of this copper corrole complex, even because of its interesting properties as a hole-transporting material in perovskite solar cells.[19]

In this paper, we investigated the sensing properties of the conductometric sensors based on polymers of [5,10,15-(4-aminophenyl) corrolato]copper (**Corr**) (**Figure 1**). The polymerization mechanism involves the oxidation of the meso-phenyl group followed by the coupling with another monomer to form a diphenylamine bridge. Further oxidation and coupling lead to the final phenazine bridge (Figure 1).

The sensor's fabrication steps are shown in **Figure 2**. The polymer is directly grown onto interdigitated electrodes to form a sensitive film filling the space between electrodes. Thus, the first challenge in this approach is to optimize the growth condition so that the polymer that starts to grow onto each electrode may form a compact film extended over both electrodes.

We found that the conductive path is established just after a minimal number of cyclic voltammetry scans. Furthermore, as we recently observed, the presence of an electron scavenger, such as the 2,6-lutidine, in the polymer precursor solution may avoid the protonation of these macrocycles.[17] Here, we investigated the effects of 2,6-lutidine on conductivity and sensitivity. Sensitivity is a figure of merit expressing the variation of the sensor response due to a change in concentration. The sensitivity is calculated as the derivative of the response curve with respect to concentration.[20]

Eventually, four corrole polymers were investigated by growing films directly onto interdigitated electrodes at different numbers of scans (20 and 40) and with or without 2,6-lutidine.

The polymers have been characterized by UV–vis spectroscopy, Scanning Electronic Microscopy (SEM), and Electrochemical Impedance Spectroscopy (EIS) to evaluate electronic properties and morphological features. The gas sensitivity was measured toward a set of Volatile Compounds (VCs) and gases.

Results show that the addition of 2,6-lutidine changes the semiconductive character from p-type to n-type. The deprotonated sensors exhibit the usual cross-selective character of corroles-based gas sensors. On the contrary, the protonated polymer exhibits high sensitivity and selectivity toward nitrogen monoxide (NO). The limit of detection of the order of tens of ppb enables the use of sensors in practical applications. For instance, in human breath, a level of less than 25 parts per billion (ppb) is expected in adults, and a level greater than 50 ppb is indicative of airway inflammation.[21] In the case of asthma, a reduction

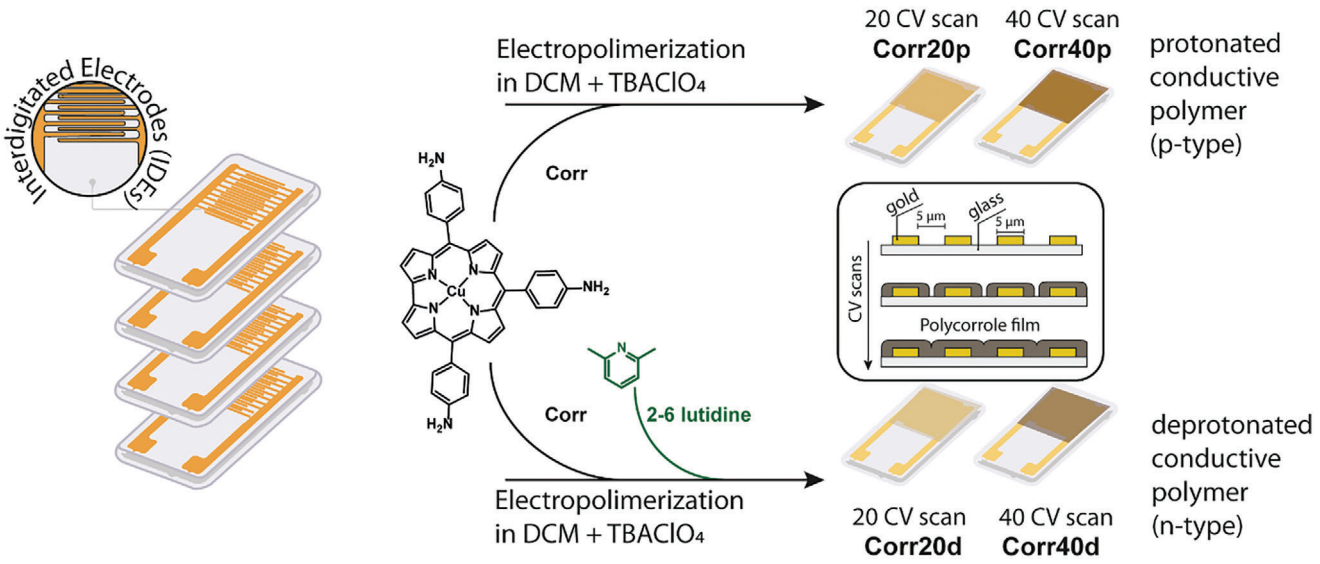

Figure 2. Schematic representation of gas sensor fabrication. **Corrole** in Figure 1A has been directly polymerized onto each interdigitated electrode. As the polymer grows, it forms a compact film connecting the electrodes, giving rise to an organic resistance. Polymers were grown from a solution of [5,10,15-(4-aminophenyl) corrolato]copper ($TBAClO_4$) in dichloromethane (DCM), deprotonated polymers can be obtained by adding 2–6 lutidine to the growth solution. Electropolymerization was carried out with twenty and forty scans. Eventually, four polymers were formed: **Corr20p** and **Corr 20d** (20 scans of protonated and deprotonated polymers), and **Corr40p** and **Corr40d** (40 scans of protonated and deprotonated polymers).

of exacerbation rate is observed in patients where the therapy is monitored by breath NO concentration.[22]

These results offer a viable procedure to process conductive polymers with highly different sensing properties.

2. Results and Discussion

2.1. Electropolymerization of Films

Sensing films were obtained through the oxidative polymerization of **Corr** monomer bearing three aminophenyl groups (Figure 1A). Figure S1A (Supporting Information) confirms that the voltammograms are compatible with previously reported data.[17] The protons developed during the oxidative polymerization process lead to the formation of a positively charged polymer with protonated quinoid species, which allows a conduction mechanism similar to that observed for polyaniline and polymers of 5,10,15,20-tetrakis(4-aminophenyl)porphyrin (see scheme in Figure S2, Supporting Information).[14]

A second series of polymers was produced by adding 2,6-lutidine to the monomer solution since a proton scavenger such as lutidine is expected to partially prevent the protonation of the polymer and the formation of the quinoid forms (see scheme in Figure S2, Supporting Information). This latter condition, important in organic heterojunctions, affects the conductive and chemical sensitivity of the polycorrole films. Figure S1B, (Supporting Information) shows the CV when lutidine is added to the monomer solution. With the increase of cycles, the oxidation peak shifts toward lower potential values, and it completely disappears at the 40th scan, leading to a significant decrease in the polymer conductivity.

As reported in ref.,[17] it is possible to tune the majority carriers from p-type to n-type by simply changing the polymerization conditions, with a potentially high impact in developing nonlinear sensing components based on this kind of polymer.

2.2. Polymeric Film Characterization

2.2.1. UV–Vis Spectroscopy

UV–vis spectroscopy was used to confirm the formation of the polymeric films onto the ITO glass surface. Figure S3A, (Supporting Information) shows the spectrum of **Corr** in CH_2Cl_2 and the 20 scans of polymer growth with and without lutidine. **Corr** shows the typical intense Soret band at 445 nm paralleled by the Q band at 570 nm. The aggregation in the polymer broadens the spectral features. Furthermore, a broad red-shifted band extended in the range 700–1000 nm supports the formation of the quinoid forms observed in the polypyrrole growth without lutidine. The UV–vis spectra features do not depend on the polymer thickness (data not shown). The spectroscopic outcomes define polymer structures, which hereinafter are indicated as **Corr20p** and **Corr40p** for the polymer growth without lutidine and **Corr20d** and **Corr40d** for that growth with lutidine assistance. Figure S3B, (Supporting Information) shows the UV–vis spectra of **Corr20p** and **Corr20d** on the IDE substrates. In this case, the absorbance of samples depends only on the material deposited on the glass between the electrodes, confirming that the polymer connects the gold electrode and is responsible for the conductivity of interdigitated sensors.

2.2.2. Sensing Film Morphologies

The morphology of the polymeric films was examined using the Scanning Electron Microscope technique. **Figure 3** reports

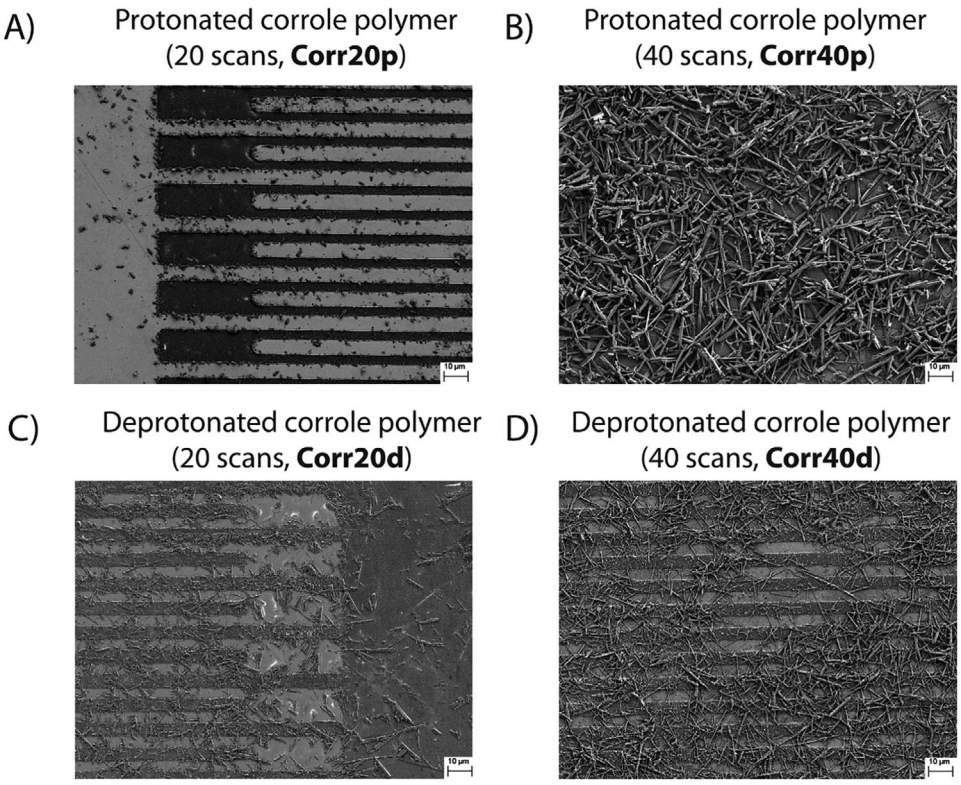

Figure 3. SEM images of A) **Corr20p** (20 scans growth protonated polymer), B) **Corr40p** (40 scans growth protonated polymer), C) **Corr20d** (20 scans growth deprotonated polymer), and D) **Corr40d** (40 scans growth deprotonated polymer), after electropolymerization onto IDE substrate. Rod-like structures are not evidenced in **Corr20p**, while they are present with different moieties in the other three cases.

the SEM analysis of the polymers after the polymerization onto IDE substrates. As shown in the case of **Corr20p**, the polymeric film fills the gap between the electrons to form a conductometric layer, which is uniform over the whole IDE surface (Figure 3A). Further magnification (Figures S4A,S5A, Supporting Information) confirms that the film mainly covers the glass between the electrodes. The film over the electrodes is characterized by nanoparticles and sporadic bigger nanostructures with more complex morphology. With the increase of scanning, the film starts to coat all the electrode surfaces with the appearance of rod-like structures, submerging the underneath IDEs (see **Corr40p**, Figure 3B). Also, in this case, higher magnification confirms the presence of film under the rods with a morphology similar to the **Corr20p** case. The sporadic structures observed in the case of **Corr20p** are likely precursors of rod-shaped elements in **Corr40p**, which increase in size with the number of scans.

The deprotonated polymer **Corr20d** morphology is shown in Figure 3C. In this case, the film is more homogenous over the gold electrode, and the rod-like elements connect the electrodes (Figure S4C, Supporting Information). The uncovered glass surface is still clearly visible. Higher magnifications (Figure S5C, Supporting Information) evidence nanoparticles onto gold electrodes, just like in the previous cases, suggesting the precursor role of these structures in the further growth of elonged elements. Finally, by increasing the number of scans to 40, the film morphology becomes closer to the case of **Corr40p**, where rods cover the film produced on the underneath IDE surface (Figure 3D; Figures S4D,S5D, Supporting Information).

The morphological results are coherent with CV curves, where the growth of rod-like nanostructures is evidenced by a decrease in current density and/or a drop and a shift of the oxidation peak. Both nanoparticles and fiber-like structures were previously reported in porphyrin derivatives, noticing that the water traces or the addition of bases, such as pyridine, produced micrometer-sized filaments,[14] justifying the presence of these structures in the presence of lutidine or at higher scanning cycles.

2.2.3. Electrical Characterization

The analysis of the electrical properties was performed using Electrochemical Impedance Spectroscopy. A typical Nyquist plot observed for the samples is reported in Figure S6 (Supporting Information), Supporting Information, which shows the case of **Corr40p** film onto IDE. In all the Nyquist plots, the complex impedance of the four sensors can be fitted by a single semicircle in the complex plane. The capacitor is replaced by a Constant Phase Element (CPE). Thus, the equivalent circuit of the sensor can be written as R0(CPE//Rs), as shown in the inset of Figure S6 (Supporting Information). R_0 is the contribution of the external circuit resistance (here, relatively small), while Rs and CPE characterize the polymer.[23] Unlike an ideal capacitor for which no energy dissipation occurs, CPE considers the energy dissipa-

Table 1. Values of Q fitted with the R_0(CPE//Rs) equivalent circuit at 5 V.

	C (nF)	CPE [n]	Rs fitted [kΩ]	R from d.c. bias at 5 V [kΩ]
Corr40p	11.24 (±3.9%)	0.87 (±0.38%)	200 (±0.91%)	197
Corr20p	0.324 (±9.19%)	0.97 (±0.72%)	10 (±0.61%)	10.3
Corr40d	13.34 (±4.17%)	0.82 (±0.4415%)	295 (±1.49%)	268
Corr20d	21.54 (±10.4%)	0.81 (±1.047%)	66 (±2.11%)	61.0

tion during the charge/discharge process.[24] A CPE element is characterized by a pseudocapacitance Q and can be related to the capacitance of the process by using the Equation (1):

$$C = \frac{(R_S Q)^n}{R_S} \quad (1)$$

where n indicates the similarity between the CPE and the ideal capacitor, for which $n = 1$.[25,26]

The values of Rs obtained by fitting EIS curves are in good agreement with the resistance measured under *d.c.* bias at 5 V. The fitted values of the equivalent circuit are shown in **Table 1**. The Nyquist plots for the polymers **Corr20p**, **Corr40d**, and **Corr20d** are reported in Figures S7–S9 (Supporting Information).

For the same number of electropolymerization cycles (20 and 40 scans), the film of protonated poly-corrole exhibits a lower resistance compared to the deprotonated ones. This behavior is expected from the cyclic voltammetry result, where lutidine addition has produced a less conductive film (see Figure S8,S9, Supporting Information). At the same time, the film resistance increases with the number of cycles for both protonated and deprotonated poly-corrole films. This behavior may appear less obvious considering, for example, that the conductance is generally proportional to the thickness of thin films.[27] On the other hand, we cannot exclude that, along with the rod-like nanostructure growth, film passivation may occur as the electropolymerization progresses, affecting the conductive properties of films, e.g., increasing resistance. As previously mentioned, this passivation behavior has already been reported in tetra-aminophenyl porphyrin polymerization in the presence of pyridine or water traces.[14] Data in Table 1 encourage this assumption since films in the presence of lutidine or with a higher number of cycles (**Corr40p**, **Corr20d**, **Corr40d**) have estimated capacitance values almost thirty times higher than **Corr20p**. Furthermore, the exponential in the CPE model is close to the ideal capacitor ($n = 1$) only in this latter case.

2.2.4. Nitrogen Oxide Sensing

The sensitivity of the four sensors was investigated by exposing the sensors to different concentrations of gases such as nitrogen oxide (NO), carbon monoxide (CO), molecular hydrogen (H_2), and volatile compounds (VCs) such as water, butanol, ethanol, toluene, and triethylamine.

All sensors show a remarkable sensitivity to NO. **Figure 4** shows the dynamics of the resistance of **Corr40p** and **Corr40d** exposed to a sequence of NO pulses at variable concentrations.

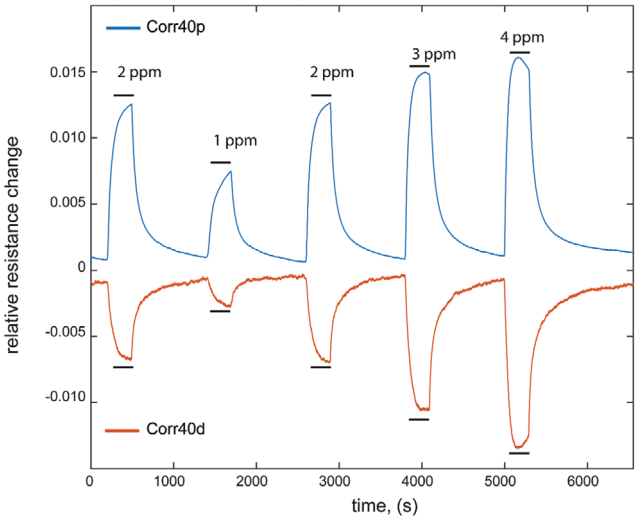

Figure 4. Sensing responses **Corr40p** (40 scans growth protonated polymer) and **Corr40d** (40 scans growth deprotonated polymer) under cyclic exposure to different NO concentrations.

Both the sensors have a fast response to the gas. As usual, the desorption is longer than the absorption, and the sensors recover the pristine baseline upon carrier gas exposure. Noteworthy, the protonation state of the polymer affects the semiconducting type, as evidenced by the fact that the two sensors show an opposite response direction to the gas: the adsorption of NO increases the resistance of **Corr40p** and decreases the resistance of **Corr40d**. Considering the electron donor character of NO, the sensor responses indicate that **Corr40p** and **Corr40d** are p-type and n-type polymers, respectively.

The quinoid structures present in **Corr40p**, also evidenced by the UV–vis spectra (see Figure S3, Supporting Information), can allow the conduction by the mechanism reported in Figure S2 (Supporting Information), inducing the p-type semiconducting character. In the case of **Corr40d**, the protonation of macrocycles is prevented by the lutidine, and then electrons in the corrole π-system confer an n-nature to the resulting polymer. The n-behavior has been previously observed in the case of poly-Fe(III)-aminophenyl porphyrin films.[28] The same considerations can be drawn for all reducing gases tested and the different number of cycles utilized for the electropolymerization. Thus, we can exclude that morphology may affect the behavior, which is instead intrinsic to the protonation state of corrole.

The sensor responses to each sample were defined as the relative resistance change:

$$\textit{relative resistance change} = \frac{R_{gas} - R_{air}}{R_{air}} \quad (2)$$

where R_{air} is the baseline resistance evaluated before the exposure to the gas, and R_{gas} is the resistance at the end of the gas exposure. **Figure 5** shows the response curves of the sensors to the test gases. Concentrations are plotted in a logarithm scale to account for the wide concentration range. The p- or n-semiconductive character observed during the exposure to NO is confirmed by the response to CO and H_2. The electron donor

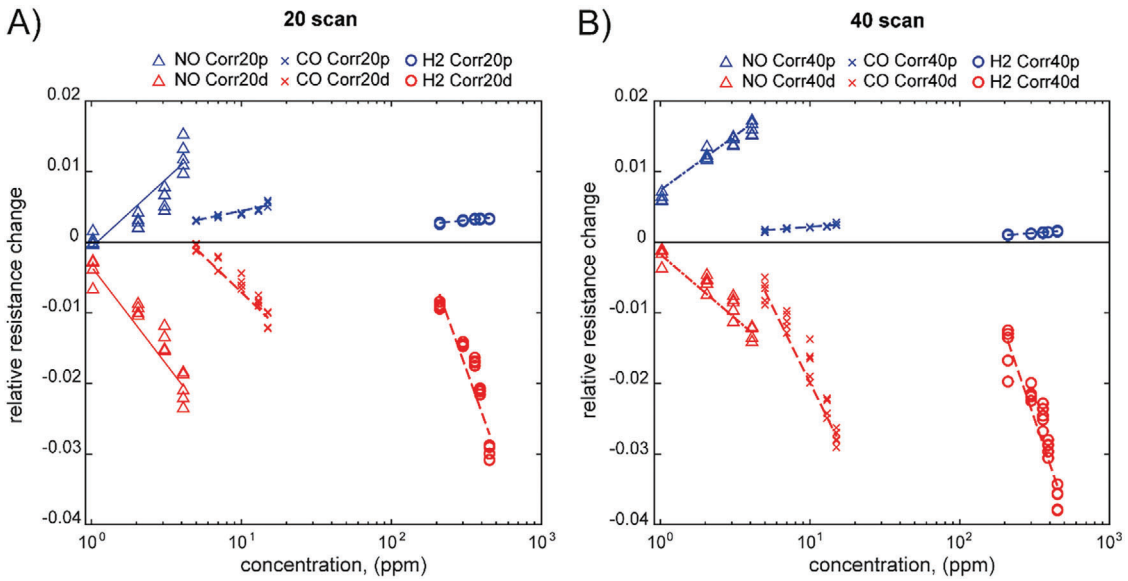

Figure 5. A) Characteristic curves of **Corr20p** (20 scans growth protonated polymer) and **Corr20d** (20 scans growth deprotonated polymer) to nitrogen oxide, molecular hydrogen, and carbon monoxide. B) Characteristic curves of **Corr40p** (40 scans growth protonated polymer) and **Corr40d** (40 scans growth deprotonated polymer) to nitrogen oxide, molecular hydrogen, and carbon monoxide. Lines report linear regressions of data.

character of H_2 is supposed to be mediated by the interaction with oxygen, suggesting an additional catalytic action of the copper corrole.[29] However, since H_2 produces lower responses than NO and CO, we did not investigate this hypothesis further in this study.

Sensors show an almost symmetrical response to NO, while, compared to CO and H_2, the deprotonated polymer shows a larger response in absolute value. Sensors at a higher number of scans displayed a slightly larger response (Figure 5B).

Figure 6 shows the response curves of the sensors to VCs. The interaction with VCs is more cumbersome than with gases: deprotonated polymers are more responsive than protonated, and, in both cases, the response is more dependent on the thickness than in the case of gases. This behavior can be explained by considering that VCs interact through multiple mechanisms and can all find suitable interaction sites in the polymer. **Corr** is characterized by hydrogen bond acceptor and donor sites, aromatic sites, and hydrophobic sites. Furthermore, VCs sorption can give rise to polymer swelling that affects the overall conductivity.

Thus, the response to VCs might depend on the intrinsic sensitivity of the monomer, the electric state of the polymer (protonated/deprotonated), and the film thickness (20/40 cycles), and the interplay of these principal causes gives rise to the different patterns of responses observed in Figure 6.

The comparison of the sensitivity provides an appraisal of the sensor response. Here, the sensitivities are calculated as the response curve slopes (first derivatives). All sensors show the largest sensitivity to NO and CO (Figure S10A, Supporting Information). The sensitivity to other compounds is orders of magnitudes smaller. The privileged affinity to NO and CO indicates the prevalence of the intrinsic sensitivity of the monomer, which is constant for all sensors, regardless of features such as protonation state and thickness. Considering the compounds of minor affinity, large differences are observed between protonated and deprotonated polymers, while the role of polymerization cycles seems less crucial, and interestingly, it is more evident for the compounds with lower sensitivity (Figure S10B, Supporting Information).

The detection limits (LODs) for NO are estimated as the ratio between the uncertainty of the relative change of resistance ($\Delta R/R$) and the absolute value of the sensitivity.[20] The uncertainty of the relative resistance changes is evaluated from the fluctuation of the resistance value measured by the multimeter and by considering the law of propagation of errors. The signal-to-noise ratio of the resistance in baseline conditions is between $4 \cdot 10^3$ (for **Corr40d**) and $5 \cdot 10^4$ (for **Corr20p**). Thus, the estimated LODs are in the order of tens of ppbs and range from 12 ppb for **Corr20p** to 90 ppb for **Corr40d**.

To investigate the possible application of this sensing material for NO detection in real cases, **Corr20p** has been exposed to NO under different relative humidity (RH) conditions, ranging from 20% to 80% (see Figure S11, Supporting Information). Remarkably, the relative resistance responses and sensitivity are improved in a wet atmosphere and stable in a wide range of relative humidity from 20% to 60% (Figure S11A, Supporting Information). Furthermore, the sensitivity is almost constant in the experimental range of humidity tested (Figure S11B, Supporting Information). These results are extremely encouraging for applying these materials as selective sensors for NO with high sensitivity, selectivity, and low dependence upon humidity as interferent.

2.2.5. Sensors in the Electronic Nose Configuration

The different sensitivity patterns toward VCs suggest that although not selective, the sensors could gain selectivity once they

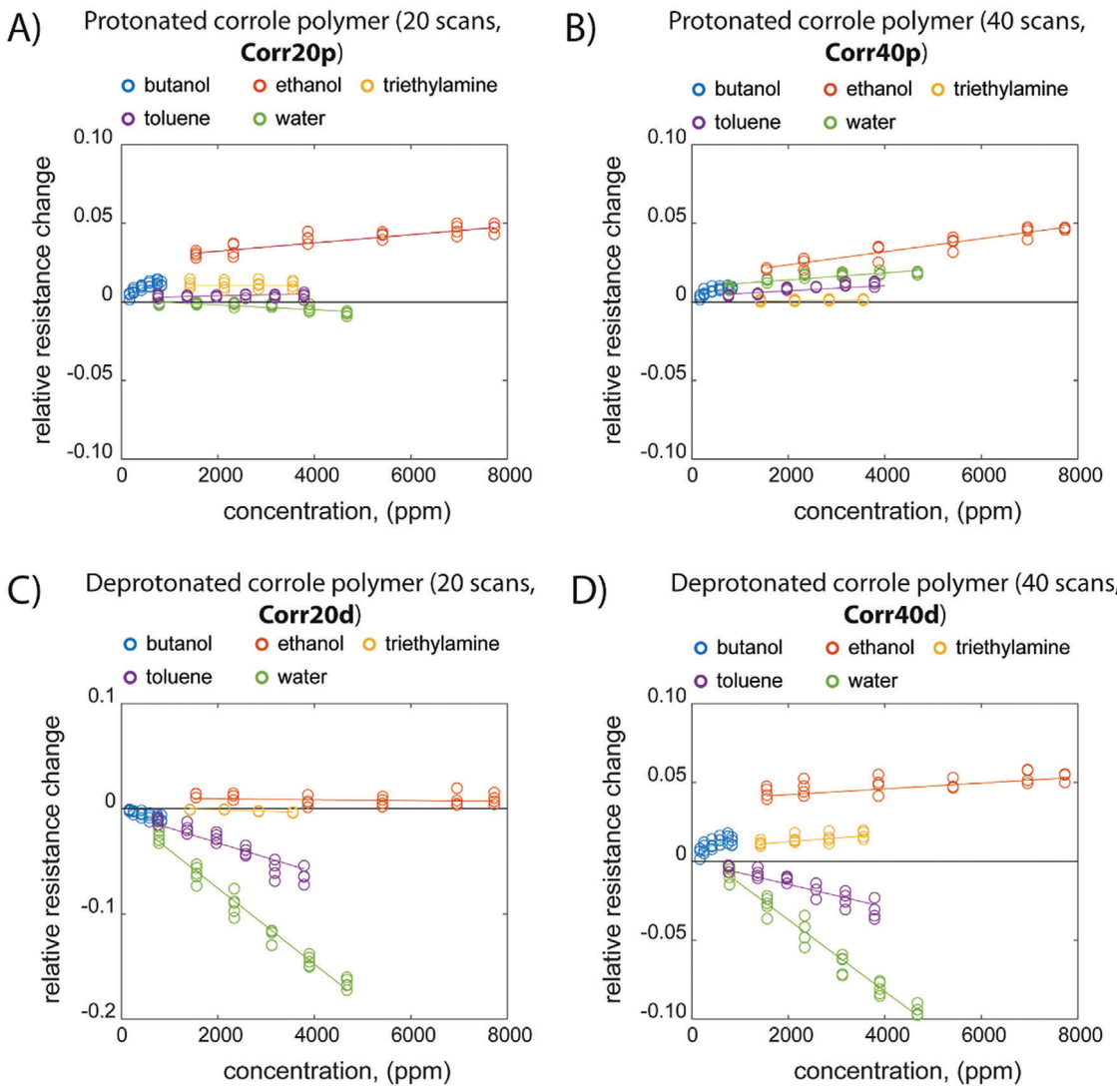

Figure 6. Characteristic curves of relative resistance change versus concentration of five volatile compounds (butanol, ethanol triethylamine, toluene, and water) of A) **Corr20p** (20 scans growth protonated polymer), B) **Corr40p** (40 scans growth protonated polymer), C) **Corr20d** (20 scans growth deprotonated polymer), and D) **Corr40d** (40 scans growth deprotonated polymer) films. Solid lines report the linear regression of data.

operate as elements in a sensor array. This concept parallels the behavior of olfaction, and it is the basic principle of electronic noses. Here, the Principal Component Analysis (PCA) has been calculated to investigate the further properties of the set of polycorrole as a sensor array. PCA is a simple and efficient algorithm that removes the correlation among sensors by defining a new orthogonal basis of uncorrelated variables. The vectors in this new basis are obtained by a linear combination of sensor data and are called principal components (PCs).[30]

To remove the effect of concentration, thus emphasizing the affinities of sensors with the test compounds, the data set has been normalized by dividing the response of each sensor by the sum of the responses of the four sensors. **Figure 7** shows the results of the PCA limiting the analysis to the first three Principal Components (PCs).

The first three principal components (PCs) account for more than 86% of the total variance of the data. The first principal component (PC1) discriminates butanol, ethanol, and triethylamine; The second principal component (PC2) accounts for the NO recognition, and the third (PC3) clusters the triethylamine separately from other compounds.

PCA evidences that, besides the individual behavior of each sensor, the cooperative response of the array provides a unique identification not only for NO but also for triethylamine, ethanol, and butanol. Surprisingly, the array does not identify CO, whose sensitivity is the closest to that of NO and larger than that of the other compounds. This behavior is dramatic evidence of the properties of sensor arrays that are not merely revealed by the properties of individual sensors but rather descend from the uncorrelated component of the sensor responses.

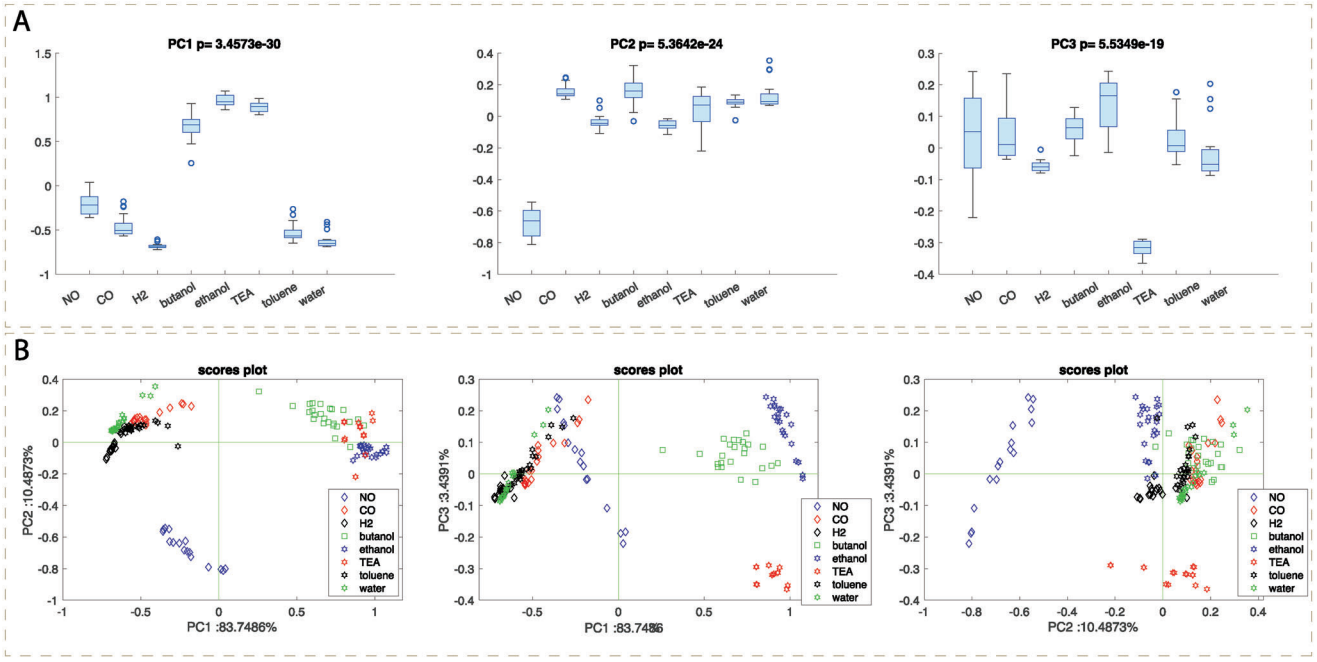

Figure 7. The results of Principal Component Analysis (PCA). A) The distributions of the tested compounds are shown, as box plots, for the first three Principal Components (PC1, PC2, and PC3). Box plots are labeled with the smallest p-value returned by a Kruskal-Wallis rank test of each class with respect to the others. B) The combinations of PC1, PC2, and PC3 are arranged in three scores-plot to represent the multidimensional arrangement of the data.

3. Conclusion

In this study, we systematically explored the preparation of copper corrole polymers through cyclic voltammetry and their utilization as conductometric gas sensors. The polymer morphological characteristics and sensing attributes exhibit a dependency on the protonation/deprotonation dynamics of corrole macrocycles during the electropolymerization process. This interplay further determines the semiconductor n- or p-type characteristics reflected in the opposite sign observed in the sensor responses.

In the case of the p-type polymers, we engineered a material of high sensitivity with a limit of detection in the range 12–90 ppb, and remarkable selectivity for nitrogen monoxide (NO) in comparison to other gases and volatile organic compounds (VOCs). These features, combined with a moderate sensitivity to humidity, make these sensors promising candidates for Nitric Oxide measurement in human breath.

Conversely, the introduction of lutidine during the electropolymerization process, designed to mitigate polymer protonation, yielded semiconducting films with n-type behavior. In comparison with the p-type device, the n-type sensor preserves, with the opposite sign, the sensitivity to NO but with a decreased selectivity. The broader pattern of sensitivity enables the use of both types of sensors in a sensor array. The Principal Component Analysis of the signals of the array shows that four sensors made of the same monomer but with two states of charge (protonated or deprotonated) can identify NO, butanol, ethanol, and triethylamine with respect to other compounds. These findings hold significant promise for advancing corrole application in gas sensors, offering a viable protocol for tailoring low-cost and low-power resistive gas sensors for specific applications.

4. Experimental Section

Reagent and Chemicals: **Corr** was synthesized according to literature methods.[4] 2,6-Lutidine (2,6-dimethylpyridine; 99%) and tetrabutylammonium perchlorate (>98%) ($TBAClO_4$) were purchased from Sigma-Aldrich.

Electropolymerization was first studied on indium tin oxide (ITO) coated glass slides (70–100 Ω^{-1}sq surface resistivity. Sigma Aldrich, Germany) having transmittance >87%, refractive index n20/D 1.517.

Sensors were prepared on gold interdigitated electrodes (IDE) on glass (model DRP-G-IDEAU5, Metrohm, Italy). IDE comprises 250 pairs of electrodes spaced by 5 µm.

Before polymerization, both substrates were sonicated in triplicate with CH_2Cl_2, acetone, ethanol, and water for 5 min at each step and dried at room temperature.

Electrochemical Deposition: Electrochemical experiments were conducted with the PalmSens3 potentiostat/galvanostat equipped with PSTrace software for Windows (PalmSens BV, The Netherlands). Polymerization was performed with a conventional three-electrodes setup, comprising either IDE or ITO as the working electrode, SCE (Saturated Calomel Electrode) as the reference, and a Pt wire as the counter electrode. Polymers were formed from a solution of 0.1 mM of **Corr** in CH_2Cl_2 with 0.1 M $TBAClO_4$ as background electrolyte and in the presence or absence of 2,6-lutidine (5 vol% solution in CH_2Cl_2). The polymerization was carried out by cyclic voltammetry (CV) from 0.1 to 0.8 V versus SCE with a scan rate of 100 mV s^{-1}. Films were formed at 20 or 40 cycles. The obtained films were rinsed with CH_2Cl_2 to remove the residues of the electrolyte and the unreacted monomers and dried in the open air in laboratory ambient conditions. Eventually, four functionalized electrodes were produced: at 20 and 40 scans without 2,6 lutidine (**Corr20p**, **Corr40p**), and 20 and 40 scans with 2,6 lutidine (**Corr20d**, and **Corr40d**).

Physical Characterization: The UV–vis spectroscopy of **Corr** in CH_2Cl_2 was conducted at micromolar concentrations due to the high molar extinction coefficient. Polymer films were deposited on ITO on glass for spectroscopical characterizations. All the spectra were recorded using a Cary 60 UV–vis Spectrophotometer in the 350–1000 nm range.

Then, microstructural characterization of polymers was carried out using field emission scanning electron microscopy (SEM, SUPRA 35, Carl Zeiss SMT, Oberkochen, Germany).

Electrochemical impedance spectroscopy (EIS) was carried out using a PARSTAT 2273 potentiostat/galvanostat. The impedance experiments were performed in a wide frequency range from 10 to 2 MHz, at an AC amplitude of 100 mV and a DC potential of 5 V. The data are analyzed with the Zsimp software.

Chemical Sensing: Sensors were placed in a tight chamber endowed with gas inlet and outlet. A synthetic air flow (20% oxygen and 80% nitrogen) was used as a reference to determine the resistance baseline, dilute the test gases, and desorb the absorbed molecules to repristinate the baseline. Sensors were exposed to different concentrations of gases: nitric oxide (NO), carbon oxide (CO), and hydrogen (H_2), and vapors: ethanol, butanol, water, toluene, and triethylamine. Test compounds were chosen in order to consider different chemical families. In the case of gases, the concentrations of analytes were provided by certified cylinders (Rivoira, Italy). For the volatile compounds, saturated vapors of compounds were obtained by means of bubblers. The compounds were always kept at 25 °C in a thermal bath to keep the saturated vapor pressure constant. Saturated vapor pressures were calculated with the Antoine equation using the parameters available in the NIST database (https://webbook.nist.gov/chemistry/ accessed on 10 October 2023). In all cases, the test concentrations were obtained by diluting either the bottle content or the saturated vapor with a flux of synthetic air. The dilution ratios were settled thanks to a Mass Flow controller system. The test concentrations of gases and VOCs are listed in Table S1 (Supporting Information). Each concentration was tested four times for each analyte, and the measurement sequence was randomically arranged.

Each measurement comprises the exposure to synthetic air to establish a constant baseline, 5 min of exposure to the sample, and the recovery in synthetic air for 15 min. The total flow rate of air in the sensor chamber was kept constant at 200 sccm. Sensor resistances were acquired in parallel by remote controlling a Keithley 2001 multimeter equipped with TCSCAN and GPIB cards; data were automatically collected on a PC and controlled by an in-house developed Matlab script. The relative resistance changes between the end of the exposure and the baseline were considered the sensor response and used in the following data analysis.

Statistical Analysis: In total, we measured 218 samples subdivided as follows: 20 samples of NO (at 4 concentrations repeated 5 times), 25 samples of CO (at 5 concentrations repeated 5 times), 25 samples of H_2 (at 5 concentrations repeated 5 times), 24 samples of toluene (at 6 concentrations repeated 4 times), 24 samples of butanol (at 6 concentrations repeated 4 times), 16 samples of triethylamine (at 4 concentrations repeated 4 times), 30 samples of ethanol (at 6 concentrations repeated 5 times) and 30 samples of water (at 6 concentrations repeated 5 times). The concentrations tested for each analyte are reported in Table S1. In the case of error bars, the plot reports mean ± standard deviation (SD). The data were autoscaled before the PCA analysis (meaning that each column had a mean = 0 and std = 1). In PCA plots, box plots are labeled with the smallest *p*-value, as returned by a Kruskal–Wallis rank test, of each class concerning the others. Here, sensitivity is defined as the slope of the curve fitting the relative response as a function of the concentration of each analyte. The error for the sensitivity is calculated with the *t*-test with a confidence bound of 95%. Data analysis was performed in Matlab 2023b using the "Statistics and Machine Learning Toolbox."

Supporting Information

Supporting Information is available from the Wiley Online Library or from the author.

Acknowledgements

The support from the Italian MUR (SUNSET PRIN2017 project #2017EKCS35) and European Union – NextGenerationEU (project ECS 0000024 Rome Technopole) is gratefully acknowledged.

Conflict of Interest

The authors declare no conflict of interest.

Data Availability Statement

The data that support the findings of this study are available from the corresponding author upon reasonable request.

Keywords

chemical sensors, corroles, electropolymers, nitric oxide, organic semiconductors

Received: January 15, 2024
Revised: April 24, 2024
Published online:

[1] A. Milone, A. Monteduro, S. Rizzato, A. Leo, C. Di Natale, S. Sub Kim, G. Maruccio, *Adv. Sustainable Syst.* **2023**, *7*, 2200083.
[2] H. Ji, W. Zeng, Y. Li, *Nanoscale* **2019**, *11*, 22664.
[3] G. S. Marks, *Q. Rev. Biol.* **1977**, *52*, 213.
[4] R. Paolesse, S. Nardis, F. Sagone, R. G. Khoury, *J. Org. Chem.* **2001**, *66*, 550.
[5] S. Nardis, F. Mandoj, M. Stefanelli, R. Paolesse, *Coord. Chem. Rev.* **2019**, *388*, 360.
[6] A. S. Hazari, S. Chandra, S. Kar, B. Sarkar, *Chem. - Eur. J.* **2022**, *28*, e202104550.
[7] J. F. B. Barata, M. G. P. M. S. Neves, M. A. F. Faustino, A. C. Tomé, J. A. S. Cavaleiro, *Chem. Rev.* **2017**, *117*, 3192.
[8] C. Di Natale, C. P. Gros, R. Paolesse, *Chem. Soc. Rev.* **2022**, *51*, 1277.
[9] G. Magna, M. Muduganti, M. Stefanelli, Y. Sivalingam, F. Zurlo, E. Di Bartolomeo, A. Catini, E. Martinelli, R. Paolesse, C. Di Natale, *ACS Appl. Nano Mat.* **2022**, *4*, 414.
[10] N. Alzate-Carvajal, A. Luican-Mayer, *ACS Omega*, **2020**, *5*, 21320.
[11] S. F. Liu, L. C. Moh, T. M. Swager, *Chem. Mat.* **2015**, *27*, 3560.
[12] L. Di Zazzo, G. Magna, M. Lucentini, M. Stefanelli, R. Paolesse, C. Di Natale, *Chemosensors* **2021**, *9*, 356.
[13] F. Bedioui, J. Devynck, B. C. Claude, *Acc. Chem. Res.* **1995**, *28*, 30.
[14] M. G. Walter, C. C. Wamser, *J. Phys. Chem. C* **2010**, *114*, 7563.
[15] N. U. Day, M. G. Walter, C. C. Wamser, *J. Phys. Chem. C* **2015**, *119*, 17378.
[16] A. Friedman, L. Landau, S. Gonen, Z. Gross, L. Elbaz, *ACS Catal.* **2018**, *8*, 5024.
[17] L. Di Zazzo, A. Kumar, R. Meunier-Prest, C. Di Natale, R. Paolesse, M. Bouvet, *Chem. Eng. J.* **2023**, *458*, 141465.
[18] A. Kumar, R. Meunier-Prest, M. Bouvet, *Sensors* **2020**, *20*, 4700.
[19] A. Agresti, B. Berionni Berna, S. Pescetelli, A. Catini, F. Menchini, C. Di Natale, R. Paolesse, A. Di Carlo, *Adv. Funct. Mater.* **2020**, *30*, 2003790.
[20] A. D'Amico, C. Di Natale, *IEEE Sens. J.* **2001**, *1*, 183.
[21] S. K. Medrek, A. D. Parulekar, N. A. Hanania, *Curr. All. Asthma Rep.* **2017**, *17*, 69.
[22] M. Essat, S. Harnan, T. Gomersall, P. Tappenden, R. Wong, I. Pavord, *Eur. Respir. J.* **2016**, *47*, 751.
[23] H. Gerengi, H. Goksu, P. Slepski, *Mat. Res.* **2014**, *17*, 255.
[24] A. Lasia, *J. Phys. Chem. Lett.* **2022**, *13*, 580.
[25] C. Sánchez-Bautista, A. J. Dos Santos-García, J. Peña-Martínez, J. Canales-Vázquez, *Solid State Ion* **2010**, *181*, 1665.
[26] A. P. Panunzi, L. Duranti, I. Luisetto, N. Lisi, M. Marelli, E. Di Bartolomeo, *Chem. Eng. J.* **2023**, *471*, 144448.

[27] D. Sharon, P. Bennington, C. Liu, Y. Kambe, B. X. Dong, V. F. Burnett, M. Dolejsi, G. Grocke, S. N. Patel, P. F. Nealey, *J. Electrochem. Soc.* **2018**, *165*, H1028.
[28] S. M. Kuzmin, S. A. Chulovskaya, M. V. Tesakova, A. S. Semeikin, V. I. Parfenyuk, *J. Porphyrins Phthalocyanines*, **2017**, *21*, 555.
[29] E. Ntagia, P. Rodenas, A. Ter Heijne, C. J. N. Buisman, T. H. J. A. Sleutels, *Int. J. Hydrogen Energy* **2016**, *41*, 5758.
[30] I. T. Jolliffe, *Principal Component Analysis*, 2nd ed., Springer, New York **2002**.